[SSC24-P2-05]

Ultra-Broadband Uncooled Infrared Camera Core for Multi-Spectral and Far-Infrared Earth, Lunar, and Planetary Observation

Francis Généreux, Francis Picard, Hélène Spisser, Alfredo Tomas, Antoine Letourneau, Bruno Fisette, Christian Proulx, Louis Martin, Timothy Pope, Christine Alain, Patrice Côté, and Patrice Topart*
INO
2740 Einstein Street, Québec, Canada, G1P 4S4; 418-559-2701
Patrice.topart@ino.ca

ABSTRACT

This paper reports on a unique solution for thermal imagery in the Earth Observation (EO) commercial space market. The High-Definition Infrared Space Camera Core (HDISCC) is based on INO's uncooled 1024x768 pixel 14 µm pitch focal plane array. The sensor can be tuned to cover spectral regions between mid-wave and far-infrared wavelengths. Current configurations include broadband mid-wave to long-wave infrared (3 µm to 14 µm) with 14 µm physical pixels, and broadband mid-wave to far-infrared (up to 100 µm wavelength with a gold black coating) with 28 µm physical pixels. In each case, stripe filters may be included in the sensor package to provide detection in multiple spectral bands. For example, in a push-broom implementation, a single camera can cover multiple mid-wave and long-wave infrared bands. The Camera Core contains the interface and proximity electronics to drive the detector, and to read out and digitize image data from the Focal Plane Array (FPA). An optional thermistor readout electronics digitizes and multiplexes up to 4 optional external thermistors to monitor the temperature for radiometric correction. The camera core was designed to withstand a 10-year lifetime in a low-Earth orbit environment. With the hundreds of EO satellites to be launched per year by 2031, this new camera core design will provide a powerful solution to reduce lead time and cost for commercial customers requiring custom multispectral infrared capability.

INTRODUCTION

Infrared imaging is transforming Earth observation applications. It offers insights into sectors like agriculture, aiding farmers in efficient irrigation and crop disease detection. It is also crucial for wildfire detection and monitoring, urban heat mapping, and monitoring land and sea surface temperature. Consequently, a growing number of companies are launching satellite constellations that provide valuable data to understand and manage these issues.[1] Uncooled cameras represent an attractive alternative to cooled solutions because of their small Size, Weight, and Power (SWaP)[2-4] and improved Mean Time Between Failures (MTBF) thanks to the absence of cryocooler.[5-7] In addition, reducing the number of cameras on board the satellite is key to reduce mass. To that end, this paper reports on a high definition, broadband detector technology that is low Earth orbit (LEO) operation compatible and covers wavelengths of mid-wave infrared (MWIR) and long wave infrared (LWIR) (e.g., 3-14 µm). This broadband sensitivity combined with the capability of adding band pass filters a few hundred microns above the focal plane array provides efficient wildfire detection and monitoring in a single camera.[8]

Furthermore, the deposition of a gold black coating atop the Focal Plane Array (FPA) extends the detector's absorption range from ultraviolet (UV) up to 100 µm. This wide spectral range covers the entire radiance reflected and emitted by the Earth as observed from top-of-atmosphere (TOA), making this type of detector particularly suitable for assessing the Earth's radiation budget.[9,10] Additionally, the detector's sensitivity in the far-infrared (FIR) region is crucial for characterizing thin ice clouds (TIC).[11] These clouds, particularly TIC2, play a crucial role in cold anomalies and hypothetically in the alteration of the polar vortex observed in the last decades.[12] Characterizing and understanding these clouds is essential for improving harsh weather forecasts.

Although uncooled bolometers are particularly well -suited for Earth Observation, a careful design of pixels is critical to achieve the required performance. INO, a Canadian center of innovation in optics and photonics has been offering custom bolometer development services for over 30 years. INO's space heritage includes the Aquarius/SAC-D mission[13,14] and the recently launched Broadband Radiometer (BBR) for the European Space Agency (ESA) Earthcare mission.[9,10,15] In this paper, various pixel architectures with pitch of 14 µm and 28 µm manufactured on a high definition 1024x768 pixel read-out integrated circuit are presented. Broadband IR sensitivity was accomplished using two schemes: a Jaumann-type pixel design[16] and a gold black coated pixel.[17] Noise Equivalent Power

(NEP) values of 5.2 pW in the MWIR and 4.2 pW in the LWIR respectively are achieved. In a pushbroom imaging configuration, multi-line averaging can significantly improve the NEP. The vacuum package design is described, largely inspired by the design from the previous LEO missions.[18,19] Finally, initial NEP results for the camera core integrating optical filters are presented.

FOCAL PLANE ARRAY

In this section, we present the performance of 3 different FPAs based on INO's readout integrated circuit. All of them can be integrated in the package presented section 3. Specifically, a 1024x768 14 µm pixel-pitch FPA, and two variations of 512x384, 28 µm pixel-pitch gold black coated FPA. Each of these FPAs is effective in the whole 2-14 µm band. With a gold black coating on the 28 µm pixel-pitch FPA, the detection band is extended to the FIR band.[20] Design variations allow to target requirements tailored to specific applications. As an example of customisation, two versions of the 28 µm pixel-pitch gold black coated FPA are presented: a fast version, with a thermal time constant around 17 ms, and a slower version with increased responsivity.

1024x768 14 µm pixel-pitch FPA

14 µm pixel-pitch FPA – Spectral response

A Jaumann absorber[15] has been implemented on active bolometers to extend their spectral response from the LWIR down to the MWIR. Figure 1 illustrates the normalized spectral responsivity, obtained using a monochromator as described in[17].

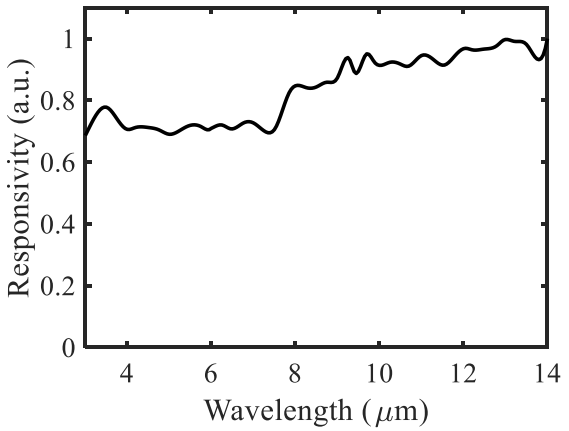

Fig. 1. Relative spectral responsivity of a 1024x768, 14 µm pixel-pitch FPA

Separate measurements at shorter wavelengths confirm that the absorption remains high down to 2 µm enabling imaging capability in the Short-wave infrared (SWIR) band if need be.

14 µm pixel-pitch FPA – NEP

To measure the NEP in different MWIR and LWIR bands, some FPAs are packaged with a Ge window in test packages. Passband filters are set sequentially in front of these detectors to enable NEP measurements across different wavelength bands. The detectors are positioned in front of a blackbody, which incorporates a thermally regulated baffle with a predefined circular aperture. By adjusting the detector distance relative to the baffle, the f-number seen by the detector can be set to 1. The experiment involves considering 4 blackbody temperatures. For each blackbody temperature, 30 frames are acquired with the aperture shutter closed and then with the shutter open. The average signal map with the shutter closed allows to remove thermal drift that may occur during the measurement. Linear regression of the resulting differential maps as a function of the temperatures yields the SiTF. The NETD is calculated by dividing the standard deviation over 30 consecutive frames by SiTF map. The NEP is evaluated by computing the irradiance incident on the detector, accounting for the baffle geometry and filter transmission, and assuming a perfectly emissive black body.

Figure 2a and 2b present NEP histograms for a typical 1024x768 FPAs in two different bands. The median NEP in MWIR band is 5.2 pW, while it is 4.2 pW in the LWIR band. The corresponding NETD value without filter is approximately 26 mK under standard conditions.

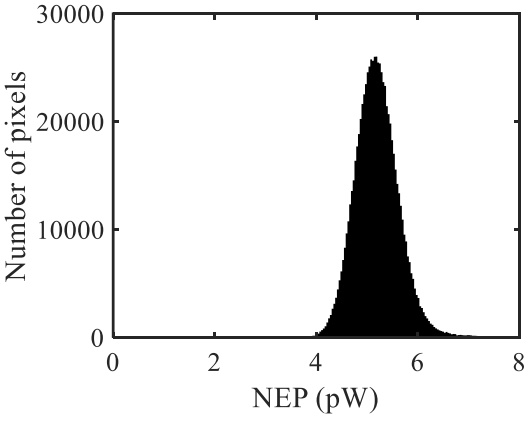

Fig.2a. NEP histogram of a 14 µm pixel-pitch FPA measured in the 3.4 µm to 4.2 µm wavelength range

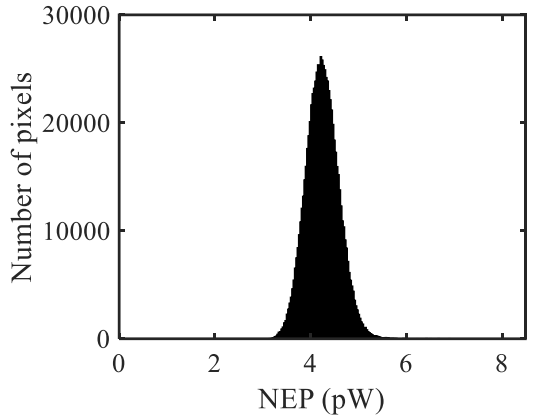

Fig.2b. NEP histogram of a 14 µm pixel-pitch FPA measured in the 10.3 µm to 12.3 µm wavelength range

14 µm pixel-pitch FPA – Thermal time constant

The pixel thermal time constant is measured using a high-speed shutter.[21] A histogram of the thermal time constant values for the pixels of the same FPA is presented in Figure 3. The median thermal time constant is 9.9 ms.

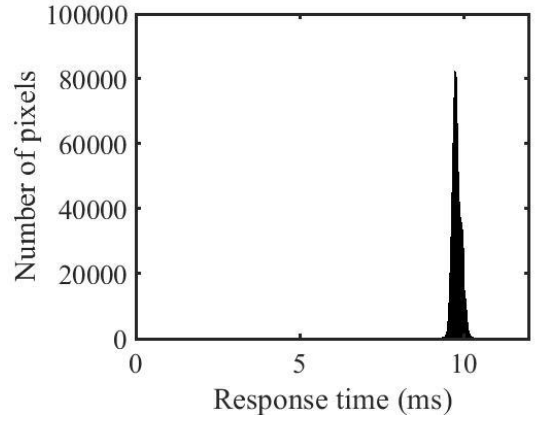

Fig. 3. Pixel thermal time constant of a 14 µm FPA

14 µm pixel-pitch FPA – Linearity

Figure 4 illustrates the average signal of a typical FPA as a function of the incoming power. The increasing irradiance has been obtained by increasing the temperature of a cavity blackbody. The differential irradiance has been chopped and measured with a calibrated pyroelectric detector. The data shows a very good linearity over a wide dynamic range. The FPA parameters can be adjusted to accommodate different dynamic ranges. In this example, a differential incident power up to 29 nW was measured, corresponding to a differential irradiance of 148 W/m^2 in the MWIR. It should be noted that the dynamic range could be further improved, if need be, by reducing the electronic gain of the FPA, with minor impact on the median NEP value.

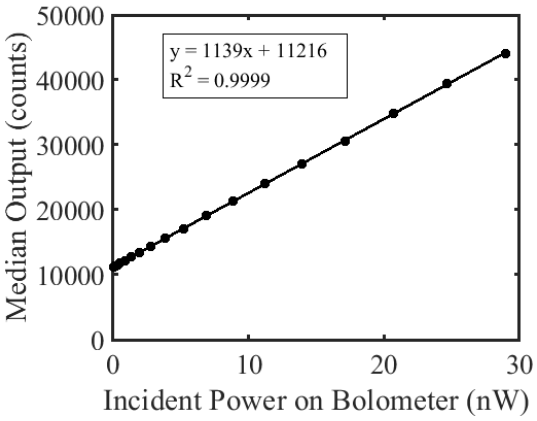

Fig. 4. FPA response with respect to power incident on each pixel

512x384 28 µm pixel-pitch FPA with Gold Black Absorber

28 µm pixel-pitch FPA - Spectral Response

Gold black coatings give pixels an extended response band up to the FIR. After the deposition, the gold black layer is trimmed[17] to maintain a high MTF. The result of trimmed gold black at a 28 µm pitch is illustrated in Figure 5. With the gold black coated FPA, the detection band is mainly limited by the windows and optics in the system, allowing for a wide range of possibilities in the choice of wavebands of interest. Furthermore, with gold black, the same FPA can be used for imaging and detection in different bands, reducing the number of cameras necessary in the payload.

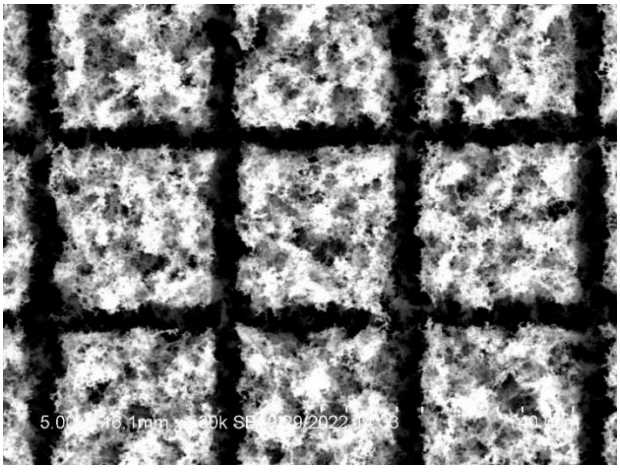

Fig. 5. Gold black layer deposited on pixels with a pitch of 28 µm and trimmed to match the pixel pitch.

Typical specular reflectance of a gold black coated substrate, as measured using a Fourier Transform IR Spectrometer, is shown in Figure 6. Reflection is lower than 10% over the entire characterized band. Assuming that diffuse reflectance is negligible in the long wavelengths, this suggests that absorption remains high up to 100 µm and beyond.

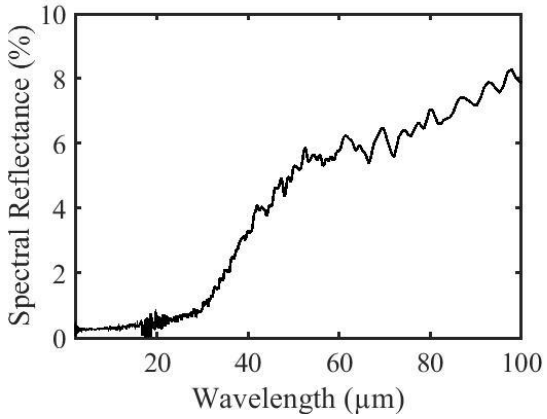

Fig. 6. Typical reflectance of a gold black coated FPA

28 µm pixel-pitch FPA - NEP

The pixel design gives the opportunity to tailor detector performances, namely the responsivity, according to the applications. Figure 7 shows the NEP histogram of a "fast" version of the 28 µm pixel-pitch gold black coated FPA. The spectral range is limited by the detector window (3-14 µm transmission). The median value is 12 pW. This NEP value is greater than that of a 14 µm pixel, but the larger collection area means that the NETD is still improved with equivalent optics. A "high-responsivity" version of the gold black coated FPA has been fabricated and measured, offering a NEP median value around 9 pW. The corresponding broadband NETDs for these 28-micron pitch pixels are about 17 mK and 13 mK respectively.

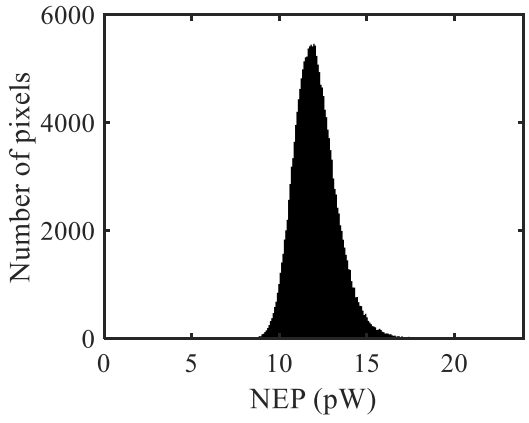

Fig. 7. NEP histogram of a "fast" gold black coated 28 µm pixel-pitch FPA

28 µm pixel-pitch FPA – Thermal time constant

The same method as in 1.1.3 is used to measure the thermal time constant of both versions of the 28 µm pixel-pitch gold black coated FPA. A histogram of the results is presented in Figure 8 for the "fast" version, exhibiting a median thermal time constant of 17 ms. The "high responsivity" version is slower, with a median thermal time constant of 25 ms.

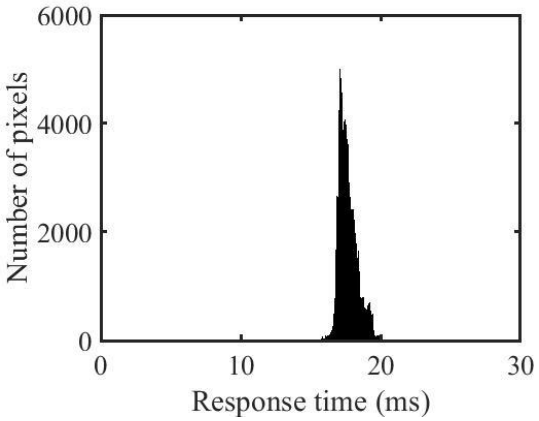

Fig. 8. Thermal time constant histogram of a "fast" gold black coated 28 µm pixel-pitch FPA

The FPA at the core of INO HDISCC can be tailored in terms of wavebands, responsivity, and thermal time constant allowing a better fit to specific applications. Three FPA variations have been presented in this section; their properties are summarised in Table 1.

Table 1. Summary of FPA performances

Typical median values	14 µm Jaumann FPA	28 µm fast gold black coated FPA	28 µm high responsivity gold black coated FPA
Pixel-pitch	14 µm	28 µm	28 µm
Waveband	2-14 µm	UV-100 µm	UV-100 µm
NEP	5.2 pW (MWIR) 4.2 pW (LWIR)	12 pW (3-14 µm)	9 pW (3-14 µm)
Thermal time constant	10 ms	17 ms	25 ms

PACKAGE

Space compatible package

Thanks to INO's space IR-detector packaging heritage, a package designed for space applications is available for the FPAs presented in section 2. Results for this package show that there is no hermiticity loss after -30°C to +70°C temperature cycling and 14 g_{rms} - vibration in

each axis. Vacuum integrity (pressure <10 mTorr) has been verified before and after temperature cycling and vibration using an INO pressure gauge[22] installed inside the package. A vacuum lifetime of greater than 10 years is expected, as similar packages fabricated in 2012[23] are still under vacuum today, as shown by measurement of their pressure gauge.

Critical components of the package assembly have been tested for radiation. FPAs with format 1024x768 and 14-µm pixel pitch have been exposed to 20 krad total ionizing dose (TID) of gamma radiation and up to 100 krad TID of protons without exhibiting NETD or operability degradation. For these tests, the FPAs were mounted in jigs representative of packages in term of radiation exposure. Similarly, package windows have been exposed to 30 krad TID of gamma radiation without any observable change of their optical properties.

Other parameters of the packaged detectors are presented in Table 2. The presented operating temperature range is for nominal performance of an FPA designed for 20°C operating temperature. The package is compatible with operation over a much wider range. Photographs of the package before and after cover sealing are presented in Figure 9 and Figure 10.

Table 2. Detector parameters

Parameter	Value
Vacuum lifetime	10 years
Detector window clear aperture	>27.5 mm (F/1, +/-30°)
Detector window transmittance (3-14 µm range)	>85% (typical 92%)
Spectral channels	custom filters for user application
Operating temperature	From +15°C to +25°C
Survival temperature	From -30°C to +70°C (MIL-STD-810 methods 501.5 and 502.5)
Random vibrations	14.1 g_{rms} (NASA GSFC-STD-7000A Table 2.4-3)
Shocks	MIL STD 883 method 2002 500G
Frame rate	30 Hz

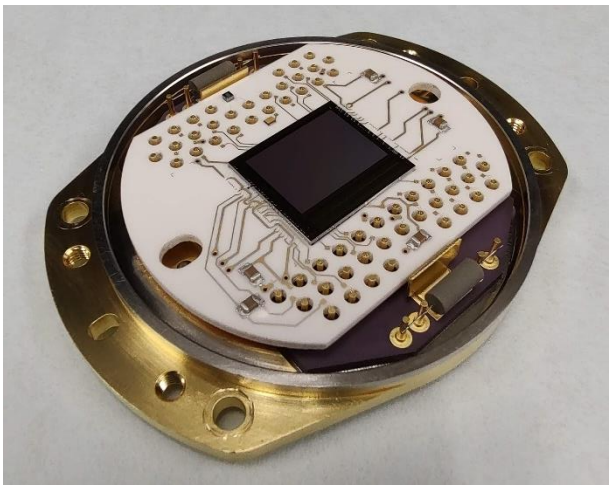

Fig. 9. Photograph of a package with FPA before cover soldering. Longest dimension is 70 mm.

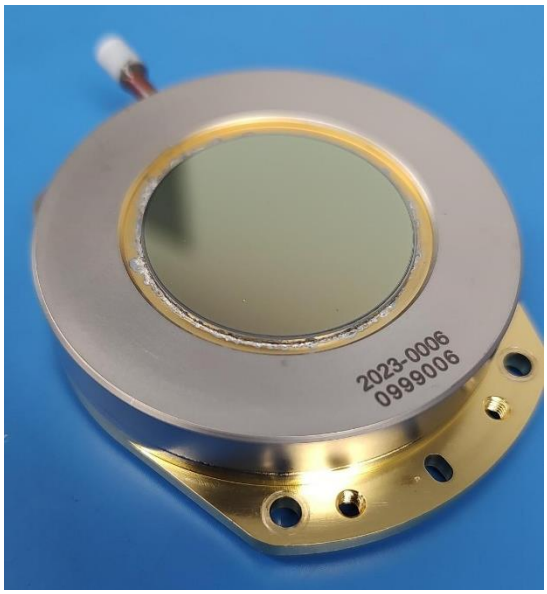

Fig. 10. Photograph of a complete package. Cover diameter is 56.8 mm.

Customized elements within the package in close proximity to the FPA

This package is designed for use with F/1 optics without vignetting with a distance between the FPA and the window large enough to accommodate an optical element right above the FPA chip (~ 500 µm). This element could be a mask, a lens, or a multiband spectral filter for example. The use of a multiband spectral filter enables push-broom multispectral imaging capabilities on a single detector.

Detectors packaged with a multiband spectral filter have already been fabricated and characterized. An example of a portion of an NEP map obtained with such a detector is presented in Figure 11. On this map, it is possible to differentiate the MWIR region, the LWIR region, as well as an "overlap region" receiving stray light from both filters and not used for imaging. In Figure 11 this overlap region is masked in black. The width of the overlap region is related to the numerical aperture of the optics and can be reduced for optical systems using smaller apertures. The packaged FPA NEPs are consistent with the tests at FPA level. In a push-broom implementation, it is, furthermore, possible to digitally average lines in each region corresponding to the same point on the ground to improve pixel sensitivity. For example, NEP below 1 pW can be achieved for both bands with the FPA used in Figure 11.

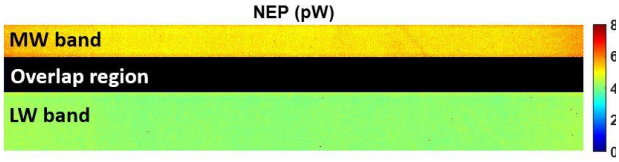

Fig. 11. Portion of a NEP map for a detector with an inner multiband filter

Alternatively, for ultra-wide band and far-infrared imaging, the detector package may be either open or equipped with a silicon or diamond window and paired with a filter wheel.

Packaged detectors are mounted on space-compatible proximity electronics to form the HDISCC camera core as described in the next section.

CAMERA CORE

The High-Definition Infrared Space Camera Core (HDISCC) is designed to support space missions requiring infrared imaging from mid-wave to far-infrared. A typical application is Earth Observation in multiple spectral bands from a LEO instrument. The HDISCC contains a packaged detector as well as interface and proximity electronics to power, read out and digitize image data from the FPA. A mock-up of the HDISCC is shown in Figure 12. The packaged detector having the proximity electronics and telemetry board underneath is placed in a mechanical housing. The latter contains connection access ports for telemetry circuit board, shutter as well as alignment features for telescope and baffle. A representative telescope is also shown. Note that the housing allows for dynamic vacuum pumping of the packaged detector if required.

The electronic components are selected based on flight heritage wherever possible. The design follows guidelines to withstand a 10-year lifetime in a low-Earth orbit environment. HDISCC can include a thermistor readout electronic circuit to read, digitize and multiplex up to 4 optional external 10K NTC thermistors. The circuit provides 20-bit digitization of thermistors. An optional external shutter can be driven by electronics external to the HDISCC via 2-wire passthrough for actuator leads. A few of the camera core characteristics are summarized in Table 3.

Table 3. Camera Core Characteristics

Parameter	Value
Output digitization	16 bit
Targeted Operational lifetime	10 years in low Earth orbit
Mass (detector, cards and housing)	1545 g
Power consumption (assuming a 5°C difference between TEC and heatsink)	1.7 W

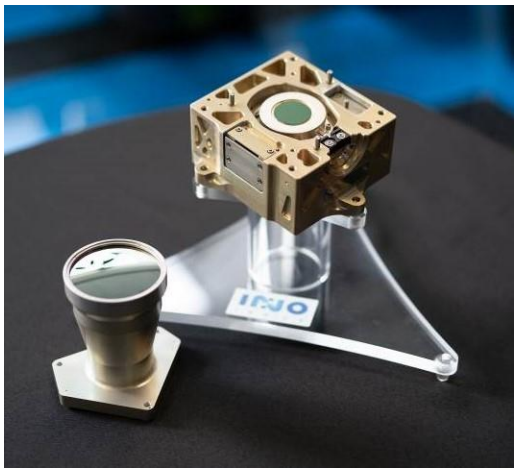

Fig. 12. Mock-up of HDISCC with its telescope

The HDISCC also went through environmental tests typical of space applications. These tests passed by the HDISCC are described in Table 4.

Table 4. HDISCC characteristics

Test	Description
Survival temperature	From -30°C to +70°C (MIL-STD-810 methods 501.5 and 502.5)
Random vibrations	14.1 g_{rms} (NASA GSFC-STD-7000A Table 2.4-3)
Shocks	200 g half-sine, 0.5 ms (ECSS-E-10-03A, 5.1.13.3)

CONCLUSION

In this paper, a broadband infrared uncooled camera core compatible with low Earth orbit operation was presented. It features filter arrays that can be custom selected and are integrated above the focal plane array thus leading to a low SWaP system. Performance results were presented for different pixel designs exhibiting NEP values in the MWIR and LWIR below 5.5 pW with

thermal time constants down to 10 ms. Due to its sensitivity in the 3 µm to 14 µm wavelength band, this camera core will be particularly useful to the growing number of satellite constellations targeting wildfire and agriculture-related measurements such as for soil and water management. Moreover, this platform enables far IR sensing with wavelengths well above 20 µm. It thus opens the door for improved forecasts of climate and weather which should contribute to better harsh climate event management. In addition to its applications in LEO, this platform could prove valuable for detecting ice water during lunar exploration missions and other extra planetary endeavours where the atmosphere is not a primary concern.

REFERENCES

1. Werner, Thermal imagery sector heats up, Spacenews, 11 July 2023, https://spacenews.com/thermal-imagery-sector-heats-up/ (accessed 23-09-23)
2. Puschell, J. J. and P. Masini, "Uncooled emissive infrared imagers for CubeSats", Proc. SPIE 9223, Remote Sensing System Engineering V, 922307, 2014, 23 September.
3. Spinhirne, J. D, R. S. Lancaster and K. R. Maschhoff, "Application and design of satellite infrared spectral imaging radiometers with uncooled microbolometer array detectors", American Meteorological Society, 11th Conference on Satellite Meteorology and Oceanography, Madison, United States, 2001, 15-18 October.
4. Fukuhara, T., T. Kouyama, S. Kato, R. Nakamura, Y. Takahashi and H. Akiyama, "Detection of Small Wildfire by Thermal Infrared Camera With the Uncooled Microbolometer Array for 50-kg Class Satellite", IEEE Transactions on Geoscience and Remote Sensing, vol. 55, no. 8, (2017) 4314-4324.
5. Deane, S., N.P. Avdelidis, C. Ibarra-Castanedo, H. Zhang, H.Y. Nezhad, A.A. Williamson, T. Mackley, X. Maldague, A. Tsourdos, P. Nooralishahi, "Comparison of Cooled and Uncooled IR Sensors by Means of Signal-to-Noise Ratio for NDT Diagnostics of Aerospace Grade Composites", Sensors, 20, (2020) 3381.
6. Uncooled infrared imaging: higher performances, lower costs, Sofradir EC, Inc., wp-uncooled-ir-imaging-v02-kp-web.pdf (lynred-usa.com) (accessed 23-09-23)
7. Uncooled detectors for thermal imaging cameras, Flir Technical note, AS_0015_EN.pdf (flirmedia.com) (accessed 23-09-23)
8. Dufour, D., L. Le Noc, B. Tremblay, M.N. Tremblay, F. Généreux, M. Terroux, C. Vachon, M.J. Wheatley, J.M. Johnston, M. Wotton, et al., "A Bi-Spectral Microbolometer Sensor for Wildfire Measurement", Sensors, 21, (2021) 3690.
9. Allard, M., L. Martin, C. Proulx, J.-P. Bouchard, P. Côté, E.-H. Oulachgar, J. Delderfield, D. Parker and F. Châteauneuf, "Current status of the EarthCARE BBR detectors development", Proc. SPIE 8176, Sensors, Systems, and Next-Generation Satellites XV, 81761E, 2011, 3 October.
10. Proulx, C., F. Williamson, M. Allard, G. Baldenberger, D. Gay, S. Garcia-Blanco, P. Côté, L. Martin, C. Larouche, S. Ilias, T. Pope, M. Caldwell, K. Ward and J. Delderfield, "The EarthCARE broadband radiometer detectors", Proc. SPIE 7453, Infrared Spaceborne Remote Sensing and Instrumentation XVII, 74530S, 2009, 1 September.
11. Blanchet, J.-P., A. Royer, F. Châteauneuf, Y. Bouzid, Y. Blanchard, J.-F. Hamel, J. de Lafontaine, P. Gauthier, N. T. O'Neill, O. Pancrati and L. Garand, "TICFIRE: a far infrared payload to monitor the evolution of thin ice clouds", Proc. SPIE 8176, Sensors, Systems, and Next-Generation Satellites XV, 81761K, 2011, 3 October.
12. Sankaré, H., J.-P. Blanchet, R. Laprise, and N. T. O'Neill. 2022. "Simulation of Arctic Thin Ice Clouds with Canadian Regional Climate Model Version 6: Verification against CloudSat-CALIPSO" Atmosphere 13, no. 2: 187. https://doi.org/10.3390/atmos13020187.
13. Pancrati, O., F. Berthiaume, F. Claveau, L. N. Phong, L. Marchese and F. Chateauneuf, "On-orbit results of the NIRST multispectral imager", 64th International Astronautical Congress, Beijing, China, 2013, September 23-27.
14. SAC-D (Satélite de Aplicaciones Científicas-D)/Aquarius Mission, https://www.eoportal.org/satellite-missions/sac-d#eop-quick-facts-section (accessed 23-09-23)
15. EarthCARE launched to study role of clouds and aerosols in Earth's climate https://www.esa.int/Applications/Observing_the_Earth/FutureEO/EarthCARE/EarthCARE_launched_to_study_role_of_clouds_and_aerosols_in_Earth_s_climate (accessed 29-06-01)
16. Du Toit, L. J., "The design of Jauman absorbers, IEEE Antennas and Propagation Magazine", vol. 36, no. 6, (1994) 17-25.
17. Généreux, F., B. Tremblay, D. Gay, S. Deshaies, M. Briand, M. Poirier, J.-S. Caron, J.-E. Paultre, D. Béland, F. Provençal, D. Desbiens, Y. Desroches and C. Alain, "Small uncooled bolometers with a broad spectral response", Proc. SPIE 10624,

Infrared Technology and Applications XLIV, 106241D, 2018, 29 May.
18. Phong, L. N., O. Pancrati, L. Marchese and F. Châteauneuf, “Spaceborne linear arrays of 512x3 microbolometers”, Proc. SPIE 8614, Reliability, Packaging, Testing, and Characterization of MOEMS/MEMS and Nanodevices XII, 86140N, 2013, 9 March.
19. Fisette, B., F. Généreux, D. Béland, P. Topart, M. Tremblay, Y. Desroches, M. Terroux, L. Marchese, C. Proulx, F. Picard, D. Dufour, A. Bergeron, F. Châteauneuf and C. Alain, “Customized packaged bolometers in niche applications at INO”, Proc. SPIE 10656, Image Sensing Technologies: Materials, Devices, Systems, and Applications V, 106560H, 2018, 14 May.
20. Ilias, S., P. Topart, C. Larouche, P. Beaupré, D. Gay, C. Proulx, T. Pope and C. Alain, “Deposition and characterization of gold black coatings for thermal infrared detectors”, Proc. SPIE 7750, Photonics North 2010, 77501J, 2010, 22 September.
21. Généreux, F., B. Tremblay, M. Girard, J.-E. Paultre, F. Provençal, Y. Desroches, H. Oulachgar, S. Ilias and C. Alain, “On the figure of merit of uncooled bolometers fabricated at INO”, Proc. SPIE 9818, Infrared Technology and Applications XLII, pp. 478-486, 2016, 20 May.
22. Sisto, M. M., S. M. García-Blanco, L. Le Noc, B. Tremblay, Y. Desroches, J.-S. Caron, F. Provencal and F. Picard, “Pressure sensing in vacuum hermetic micropackaging for MOEMS-MEMS”, J. Micro/Nanolith. MEMS MOEMS 9(4) (2010), 041109.
23. Fisette, B., C. Chevalier, A. Lépine, M. A. Boucher, C. Larouche, M. Tremblay, D. Lemieux, L. P. Tremblay, D. Dufour, Y. Desroches, P. Topart and F. Châteauneuf, “Design and fabrication of a scalable high-reliability vacuum sealed package for infrared detectors”, 2012 4th Electronic System-Integration Technology Conference, Amsterdam, Netherlands, pp. 1-6, 2012.